Stress Accumulation and Earthquake Activity on the Great Sumatran Fault, Indonesia

Muhammad Taufiq Rafie
Institut Teknologi Bandung
David P. Sahara (david.sahara@gf.itb.ac.id)
Institut Teknologi Bandung https://orcid.org/0000-0003-1785-8962
Phil R. Cummins
Australian National University
Wahyu Triyoso
Institut Teknologi Bandung
Sri Widiyantoro
Institut Teknologi Bandung

Research Article

Keywords: Coulomb stress changes, forearc sliver, oblique subduction, Great Sumatran Fault, megathrust earthquakes

Posted Date: January 4th, 2022

DOI: https://doi.org/10.21203/rs.3.rs-1195020/v1

Version of Record: A version of this preprint was published at Natural Hazards on January 17th, 2023.
See the published version at https://doi.org/10.1007/s11069-023-05816-2.

Abstract

The seismically active Sumatra subduction zone has generated some of the largest earthquakes in the instrumental record, and both historical accounts and paleogeodetic coral studies indicate such activity has historical recorded megathrust earthquakes and transferred stress to the surrounding, including the Great Sumatran Fault (GSF). Therefore, evaluating the stress transfer from these large subduction earthquakes could delineate the highly stressed area as potential-earthquake region along the GSF. In this study, we investigated eight megathrust earthquakes from 1797 to 2010 and resolved the accumulated Coulomb stress changes onto the 18 segments along the GSF. Additionally, we also estimated the rate of tectonic stress on the GSF segments which experienced large earthquake using the case of: (1) no sliver movement and (2) with sliver movement. Based on the historical stress changes of large earthquakes and the increase in tectonic stress rate, we analysed the historical stress changes time evolution on the GSF. The Coulomb stress accumulation of megathrust earthquakes between 1797-1907 increase the stress changes mainly on the southern part of GSF which followed by four major events between 1890-1943. The estimation of tectonic stress rates using case (1) produces low rate and long recurrence intervals which implies that the megathrust earthquakes plays an important role in allowing the GSF earthquake to occur. When implementing the arc-parallel sliver movement of case (2) to the calculation, the tectonic stress rates is 9 to 58 times higher than case (1) of no sliver movement. The observed slip rate of 15-16 mm/yr at the GSF is consistent with the recurrence interval for full-segment rupture of 100-200 years obtained from case (2). This suggests that the GSF earthquake is more controlled by the rapid arc-parallel forearc sliver motion. Furthermore, the analysis of stress changes time evolution model shows that some segments such as Tripa (North and South), Angkola, Musi and Manna appear to be brought back in their seismic cycles since these segments have experienced full-segment rupture and likely locked, increasing their earthquake hazard potentials.

1. Introduction

The Sumatran subduction zone is the world's most classic example of oblique, partitioned subduction (Fitch 1972; Jarrad 1986), in the sense that it involves a consistent regime of oblique convergence, with trench-parallel component partitioned between the Sumatra megathrust and the Great Sumatra Fault (GSF), extending over 1900 km. The GSF is a mature fault, with total offset of at least 20 km and about 15 mm/yr dextral slip (Sieh and Natawidjaja 2000), which cuts across the island of Sumatra for 1900 km. The GSF has a history of generating large earthquakes, with over 19 earthquakes of magnitude 6.5 or greater having occurred since 1892 (Hurukawa et al. 2014), the largest being a multi-segment rupture of magnitude 7.6. However, now earthquake of magnitude greater than 7 has occurred since 1950, prior to Indonesia's explosive growth in population during the latter half of the 20th century. Because the GSF is in some places proximate to dense population centers, GSF earthquakes pose a significant threat to lives and infrastructure, and it is therefore important to understand the fault's seismogenic potential.

The large GSF earthquakes in the early part of the 20th century followed a suite of great Sumatra megathrust earthquakes that occurred throughout the 20th century. While any connection between

Sumatra megathrust earthquakes and GSF seismicity has not been firmly established, connections between megathrust and forearc activity have been established in other oblique subduction zones like SW Japan (Hori and Oike 1996; Mitogawa and Nishimura 2020; Shirakura et al. 2014), where the stress perturbations associated with the megathrust earthquake cycle can create temporal “windows” during which the stress regime is more favourable to the occurrence of forearc earthquakes. Such a mechanism was proposed for earthquakes along the northern part of the GSF following the Great 2004 Sumatra-Andaman megathrust earthquakes (McClosky et al. 2005). Despite the subsequent occurrence of several great earthquakes along the Sumatran megathrust during 2005-2010, this sequence has not yet been followed by any GSF earthquakes of magnitude greater than 6.6.

In this study, we considered the Coulomb stress accumulation on the GSF prior to the 2004 Sumatra Andaman earthquake. We implement heterogeneous co-seismic slip models of each large megathrust earthquake to calculate the coseismic stress perturbation, as well as a model for tectonic stress due to the coupling of the obliquely convergent plate motion at the Sumatra megathrust. We consider two cases: (1) no movement of the forearc sliver, so as to facilitate comparison with other forearcs in obliquely convergent margins and (2) with movement of the forearc sliver that is consistent with recent Global Positioning System (GPS) measurements of surface velocities in the forearc. Using the historical stress changes of large earthquakes and the rate of increase in tectonic stress, we estimate the time evolution of stress changes on the GSF, with a view to better understanding its potential to produce large, damaging earthquakes.

2. Oblique Subduction And Forearc Slivers: Sumatra Compared With Sw Japan

Almost all the world’s subduction zones involve some degree of oblique convergence. These often exhibit convergence partitioning, with arc-perpendicular and some arc-parallel convergence taken up on the megathrust, while the remaining component of arc-parallel convergence is taken up by strike-slip faults in the upper plate, often near the volcanic arc (Fitch 1972; Jarrad 1986; McCaffrey 1992). The crustal block between this strike-slip fault system and the trench is called a forearc sliver, and may migrate along strike in the direction of arc-parallel convergence. Almost all forearc slivers are buttressed at their leading edge, however, which hinders along-strike movement and leads to a dominantly trench-parallel compressive stress field in the forearc sliver (Beck et al. 1993; Wang 1996).

The Nankai Trough, where the Philippine Sea Plate converges with SW Japan at a rate of 59-65 mm/yr and obliquely of 20^{o}, has one of the world’s best-studied forearcs. Although similar in some ways to Sumatra, it is also a useful benchmark that is typical of oblique subduction zone forearcs worldwide. The arc-parallel component of convergence at the Nankai Trough is partitioned between the trough and a dextral fault system that cuts through SW Japan over a distance of over 500 km, from Kyushu to the Kii Peninsula, known as the Median Tectonic Line (MTL). The forearc sliver between the trough and the MTL migrates westward in the direction of arc-parallel convergence at a rate of 5-10 mm/yr (Tabei et al. 2003). The subduction plate boundary rotates counter-clockwise offshore Kyushu, creating a geometric buttress

(Beck et al. 1993) that is consistent with the arc-parallel compression in SW Japan inferred from focal mechanism data (Wang 2000). The MTL is the longest onshore fault in Japan, consisting of 12 segments separated by gaps, bends, etc., and paleoseismic evidence indicates a recurrence interval of 1000-3000 years, with relatively high slip (5-8 m) events suggestive of multi-segment rupture (Tsutsumi and Okada 1996). Given that almost all forearcs are buttressed (Beck 1991; Wang 1996) and there are very few examples large, strike-slip earthquakes on forearc-sliver-bounding faults worldwide, we regard this the low rate of arc-parallel movement and long earthquake recurrence time as typical of forearc slivers in obliquely convergent subduction zones.

While the Sumatra subduction zone is similar to SW Japan in being an ocean-continent subduction zone with the same rate and obliquity of convergence (about 41-62 mm/yr and 20^{o}, respectively), its forearc sliver and the GSF that bounds it differ in ways that make it unique among forearc slivers worldwide. At 1900 km length, it is the longest active strike-slip fault in the world, although its 18+ segments and total offset of 20 km (or possibly more, see Sieh and Natawidjaja 2000) fall in the middle of the range of major strike-slip faults (Stirling et al. 1996). Unlike almost all other forearc slivers, the Sumatran forearc is unbuttressed with its movement along the arc-parallel direction of convergence accommodated by spreading in the Andaman Sea (Curray 2005; Kimura 1986). This is supported by the forearc stress orientations estimated by Rafie et al. (2021), who found that the principle horizontal compressive stress in the Sumatra forearc is oriented in the direction of plate convergence, rather than being arc-parallel as it would for a buttressed forearc. It was long thought that the slip rate along the GSF decreases from 25 mm/yr near the equator to only 6 mm/yr near the Sunda Strait (McCaffrey 1991), which seemed to be consistent with both geodetically and geologically measured slip rates (Genrich et al. 2000; Sieh and Natawidjaja 2000), respectively) and implied arc-parallel extension of the forearc sliver. However, more recent work on both geologically and geodetically determined slip rates now suggest that these data can be fit with a uniform slip rate of about 15 mm/yr (Bradley et al. 2017; Natawidjaja et al. 2017). In particular Bradley et al. (2017) show that the geodetic data are consistent with along-arc movement of the forearc sliver by 15 mm/yr, 1.5-3 times faster than the SW Japan sliver.

The greatest contrast between the GSF and the MTL, and other forearc slivers worldwide, is in its level of earthquake activity. While the MTL has not experienced a large, destructive earthquakes since at least 1600 AD (Tatsumi and Okada 1996) and possibly longer, the GSF has experienced at least 20 earthquakes of magnitude $\geq$ 6.5 (Table 1 and Hurukawa et al. 2014) since 1892, many of which caused widespread damage. When the greater fault length but shorter historical record are taken into account, this amounts to more than an order of magnitude greater the number of large earthquakes per year and km of fault length on the GSF vs. the MTL. In Table 1 we have used the average slip- and rupture area-magnitude relationships of Wells and Coppersmith (1994) to estimate slip and rupture area for these large, historical GSF earthquakes. For those earthquakes that involve full-segment rupture (fractional area > 60%), the average slip varies between 1.8 and 3.3 m. Considering the 15 mm/yr average slip rate obtained by Bradley et al. (2017), a slip-predicable earthquake recurrence model would suggest

recurrence times of 120-220 years, again an order of magnitude more frequent than paleoseismic estimates of recurrence times for the MTL.

Table 1

Segment geometry and average slip and stress drop estimates for large (M≥6.5) GSF earthquakes. Magnitude estimates are taken from Hurukawa et al. (2014). Slip is determined using the average slip-magnitude relationship of Wells and Coppersmith (1994). Fractional area reflects the ratio of rupture area estimated from Wells and Coppersmith (1994) divided the area of the segment, assuming a downdip rupture width of 20 km. Stress drops are calculated using the formula for strike-slip faults of Kanamori & Anderson (1975), again assuming a downdip width of 20 km and a rigidity of 32 GPa. Creeping segments are identified from Ito et al. (2012), Natawidjaja (2018a) and Tong et al. (2018). Where a segment has not experienced and earthquake, knowledge of its seismogenic potential is indicated by “creeping”, “unknown” or, in the case of Barumun, “stress shadowed”, indicating it has been affected by the 1892 earthquake in the adjacent Angkola segment.

No	Segment	Length	Strike	Historical earthquake Year	Mag	Slip (m)	Fractional Area (%)	Δτ(MPa)
1	Seulimeum	148	148	1964	6.7	0.5	14	0.5
2	Aceh	200	135	Creeping (Ito et al., 2012 and Tong et al., 2018)				
3	Tripa North	101	114	1935	7.0	1.0	38	1.0
4	Tripa South	108	144	1936[2]	7.2	1.4	53	1.5
				1990	6.7	0.5	19	0.5
5	Renun	175	140	1921	6.8	0.6	14	0.6
6	Toru	52	152	Unknown				
7	Angkola	170	145	1892[2]	7.5	2.7	63	2.7
8	Barumun	152	144	Stress Shadowed				
9	Sumpur	45	163	Unknown				
10	Sianok	79	149	1926	6.5	0.3	17	0.3
11	Sumani	45	142	1926	6.8	0.6	56	0.6
				1943[1,2]	7.6	3.3	102	3.4
12	Suliti	84	147	1943[1,2]	7.6	3.3	102	3.4
13	Siulak	73	148	1909[2]	7.3	1.8	97	1.8
				1995	6.7	0.5	28	0.5
14	Dikit	69	141	2009	6.6	0.4	24	0.4
15	Ketaun	83	141	1943[2]	7.3	1.8	85	1.8
				1952	6.8	0.6	30	0.6
16	Musi	68	145	1900	7.0	1.0	56	1.0

No	Segment	Length	Strike	Historical earthquake Year	Mag	Slip (m)	Fractional Area (%)	Δτ(MPa)
				1979	6.5	0.3	20	0.3
17	Manna	77	135	1893	7.0	1.0	49	1.0
18	Kumering	153	131	1933[2]	7.5	2.7	70	2.7
				1994	6.8	0.6	16	0.6
19	Semangko	87	142	Unknown				
[1] This 1943 earthquake was multi-segment and fully ruptured both Sumani and Suliti segments								
[2] Full downdip width assumed to have ruptured when the fractional area > 50%								

3. Influence Of Sumatra Megathrust Earthquakes On Gsf Earthquake Activity

In low-stress forearcs like SW Japan and Sumatra, large megathrust events can cause stress perturbation sufficient to alter the orientations of principle stress axes (Rafie et al. 2020; Wang 2000), and thereby alter earthquake activity in the forearc. In SW Japan, changes in shear stress on the inland faults caused by great megathrust earthquakes drive temporal variations in seismicity in the SW Japan forearc, modulating the occurrence of large shallow crustal earthquakes in the forarc so that their frequency is greatest 50 years before and 10 years after the occurrence of megathrust earthquakes (Hori and Oike 1999; Mitogawa and Nishmura 2020; Shikakura et al. 2014). Similar perturbations to the forearc stress field due to the Great 2004 Sumatra-Andaman earthquake caused changes in seismic activity in the Andaman Sea (Sevilgen et al. 2012), and likely brought forward the next rupture of the northern part of the GSF (McClosky et al. 2005).

Sumatra forearc stress is likely to be influenced by an extensive history of large Sumatra megathrust earthquakes. Since the beginning of the 21st century, the Sumatra subduction zone has recorded some of world's largest instrumentally recorded megathrust earthquakes. Historical accounts describe similar level of earthquake activity extending over the past 225 years (Newcomb and McCann 1987; see Fig. 1), and coral paleogeodetic and paleotsunami studies extend a similar record to the early Holocene (Philibosian et al. 2014; Rubin et al. 2017). A series of historical events occurred during the colonial period: 1797 Mw ~8.7 (Natawidjaja et al. 2006), 1833 Mw ~8.9 (Natawidjaja et al. 2006), 1861 Mw ~8.5-8.6 (Briggs et al. 2006; Meltzner et al. 2015; Natawidjaja et al. 2006), and 1907 Mw ~8.2-8.4 (Martin et al. 2019). No large Sumatra megathrust earthquakes were experienced through the rest of the 20th Century, until a series of very large events at the beginning of the 21st : 2004 Mw 9.1 Sumatra-Andaman (Ammon et al. 2005; Rhie et al. 2007), 2005 Mw 8.6 Nias-Simeulue (Konca et al. 2007), 2007 Mw 8.4 Bengkulu (Konca et al. 2008), 2010 Mw 7.8 Mentawai (Yue et al. 2014).

As described above, the GSF also has an extensive history of large earthquakes (Table 1 and Hurukawa et al. 2014; Natawidjaja and Triyoso 2007; Newcomb and McCann 1987). Soon after the initiation of a sequence of major megathrust earthquakes between 1797-1907, some large GSF earthquakes were observed (Fig. 2). The delays between the occurrences of major events along GSF and nearby (within 500 km) megathrust earthquake are presented in Fig. 3. Following Natawidjaja et al. (2006), we divided GSF into two areas: northern (Seulimeum to Angkola) and southern (Sumani to Kumering). The histograms of the time intervals between the occurrence of each GSF earthquake in Table 1 and all preceding megathrust events that occurred with 500 km of the GSF event show that, for the northern GSF earthquakes, 11 out of 16 time intervals are 150 years or less. For the southern GSF earthquakes, all 25 time intervals are in the range 50-250 years. This clustering of time intervals between GSF and megathrust earthquakes suggests that megathrust events modulate earthquake activity on the GSF.

4. Data And Methods

The best way to study the interaction of the effects of megathrust strain accumulation and rupture on inland faults is by modelling changes in forearc stress, as has been considered by studies of the Nankai Trough (Hori and Oike 1999; Mitogawa and Nishmura 2020; Shikakura et al. 2014), Cascadia (Wang 2000), Chile (Ryder et al. 2012) and Caribbean (ten Brink and Lin 2004) forearcs.

To analyse the occurrence of large earthquakes along the GSF and investigate whether and if so, how they might be influenced by major megathrust earthquakes, we used the catalogue of Hurukawa et al. (2014) to provide precise hypocenter locations of large earthquakes $M \geq 7.0$ and their fault planes since 1892. The GSF was segmented into 19 segments by Sieh and Natawidjaja (2000), and these were used by Hurukawa et al. (2017) and other studies of the GSF. Although the National Center for Earthquake Studies of Indonesia (PUSGEN 2017) detailed the GSF segmentation into 41 sub-segments, we prefer the simpler 19-segment model, and we have excluded the Sunda segment (Fig. 2). Also, we have ignored the short-thrust segment in the northernmost 30 km of the Tripa segment as specified by PUSGEN (2017), so that we can consider the entire GSF as a vertical strike-slip fault. Further refinement of fault geometry could be considered in future work, but for the present study we want to focus on a simple model for GSF earthquake activity.

5. Estimation Of Change In Coulomb Failure Stress Due To Great Megathrust Earthquakes

The Coulomb failure criterion describes the stress condition under which a pre-existing fault can rupture, and relates the shear stress on the fault to the normal stress (King et al. 1994). The static Coulomb Failure Stress change (ΔCFS) is often implemented to explain the spatial pattern of aftershock occurrence or subsequent triggered events caused by a large earthquake (e.g., King et al. 1994; Stein 1999; Toda et al. 1998, 2005). ΔCFS is defined as:

$$\Delta CFS = \Delta\tau + \mu(\Delta\sigma + \Delta P)$$

1

Where $\Delta\tau$ is the shear stress change on the fault (positive in the slip direction), μ is the fault friction coefficient, $\Delta\sigma$ is the change in normal stress (positive in extension) and ΔP is the pore pressure change. $\Delta\tau$ and $\Delta\sigma$ arise from the perturbation to the regional stress field caused by a large earthquake. The change in pore pressure is often related to mean stress change and assumed to be proportional to the normal stress change, so that equation (1) is usually replaced by:

$$\Delta CFS = \Delta\tau + \mu'\Delta\sigma$$

2

Where μ' is called the apparent or effective friction coefficient which includes changes in pore pressure. Assuming the secular change in tectonic stress is such that the stress on a fault will accumulate to a level resulting in rupture, a positive ΔCFS will bring the fault closer to failure than it was prior to the large earthquake, while a negative ΔCFS will lengthen the time it takes for the accumulation of stress to lead to rupture (Harris 1998). We use the COULOMB 3.4 code (Lin and Stein 2004; Toda et al. 2005) to calculate ΔCFS using the elastic dislocation approach (Okada 1985, 1992) for eight historical Sumatra megathrust events. The Coulomb stress calculations are then estimated for the specific orientation of each of the 18 segments of the GSF considered here.

The ΔCFSs caused by the megathrust earthquakes were calculated based on the slip distributions of historical megathrust earthquakes. The rupture model of each large earthquake was obtained from previous studies (Table 2). The slip models of the 1797 and 1833 earthquakes were taken from Natawidjaja et al. (2006) which was constructed based on coral microatoll measurements. We take the slip distribution of the 2005 Nias-Simuelue as an analog for that of the 1861 earthquake, since both earthquakes have similar patterns of coseismic uplift measured from corals (Meltzner et al. 2015). The 1907 slip distribution is obtained from the macroseismic, seismological, and tsunami observations of Martin et al. (2019). The rupture model of the 2004 Sumatra-Andaman earthquake was taken from Rhie et al. (2007) which applied finite fault inversion of long-period global seismic waveforms and GPS-measured coseismic displacement. The rupture models of 2005 Nias-Simeulue, 2007 Bengkulu, and 2010 Mentawai earthquakes were taken from Hayes (2017) which employed finite fault inversion of both body- and surface waves. The rupture models for the post-2004 earthquakes were accessed through the SRCMOD-earthquake source model database (Mai and Thingbaijam 2014).

Table 2
Lists of historical large interplate earthquakes recorded in Sumatra subduction zone

List historical earthquake	Mw	Slip model used for ΔCFS models
1797 Sumatra	~8.7	Natawidjaja et al. (2006)
1833 Sumatra	~8.9	Natawidjaja et al. (2006)
1861 Sumatra*	~8.5-8.6	Slip of 2005 Nias-Simeulue earthquake
1907 Sumatra	~8.2-8.4	Martin et al. (2019)
2004 Sumatra-Andaman	~9.1	Rhie et al. (2007)
2005 Nias-Simeulue	~8.6	Hayes (2017)
2007 Bengkulu	~8.4	Hayes (2017)
2010 Mentawai	~7.8	Hayes (2017)

* The slip distribution of 2005 Nias-Simeulue earthquake is used as slip model of the 1861 Sumatra earthquake since both earthquakes produced similar ruptures on the Nias-Simeulue patch (Meltzner et al. 2015).

We calculated the ΔCFS caused by these eight historical megathrust earthquakes on each GSF segment, which we henceforth denote as ΔCFS_m. As has been presented in previous studies (e.g., Mildon et al. 2016 and Mildon et al. 2019), the Coulomb stress calculation is most sensitive to the variation of strike. Therefore, for bending fault of Angkola and Barumun segments, we treated the segments by dividing their geometry into two-parts: from initial fault to the bending point and from bending point to the other end of fault.

Cattin et al. (2009) studied how variations in seismicity in the Sumatra-Andaman-Sagaing fault system might be caused by the stress perturbations due to the 2004 and 2005 megathrust earthquakes, but were unable to constrain the effective friction of the GSF. The effective friction coefficient value we used for all segments was 0.1, because this is consistent with many studies of the SW Japan forearc (Iio 1997; Hori and Oike 1999; Shikakura et al. 2014; Mitogawa et al. 2020), as well as with studies of major crustal strike-slip faults (Carpenter et al. 2015; Provost et al. 2003; Townend and Zobak 2006). We calculated ΔCFS_m at 10 km depth. This choice of depth is supported by previous studies which showed that the stress changes on the GSF are relatively constant from 10 to 30 km depth (Cattin et al. 2009; Qiu and Chan 2019). From the calculated ΔCFS_m, we investigated the effect of stress transfer with the occurrence of major earthquakes along the GSF. The results for ΔCFS_m calculated on the GSF segments due to each large Sumatran megathrust earthquake are shown in Fig. 4.

The ΔCFS_m distribution on the GFS due to the 1797 earthquake (Fig. 4a) has negative values around the central part of the GSF, especially the Toru, Angkola and Barumun segments. Positive values for ΔCFS_m of > 0.1 MPa are found southward from Sumpur to Dikit. As for the 1833 earthquake (Fig. 4b), similar

positive and negative stress transfers southward and northward, are found, respectively. The 1907 earthquake (Fig. 4c) caused a slight positive ΔCFS_m of ~ 0.01 MPa on the Tripa to Angkola and Barumun segments, and a negative ΔCFS_m of ~ -0.01 MPa on northern part of the GSF. Due to its high stress release, the 2004 Sumatra-Andaman earthquake (Fig. 4d) caused a significant increase of ΔCFS_m on the northern part of the GSF of ~0.4 MPa. The 2005 Nias-Simeulue earthquake (Fig. 4e), on the other hand, showed a positive and negative ΔCFS_m of ~ 0.1 MPa in magnitude at the southern and northern parts of the Tripa segment, respectively. The 2007 Mentawai earthquake (Fig. 4f) caused peak ΔCFS_m of 1.0 MPa on the Musi and Manna segments, which decreased gradually southward down to -0.01 MPa in the Semangko segment. Negative ΔCFS_m as low as -0.7 MPa was modelled in the Dikit segment and continued northward to ~ -0.04 MPa in the Sianok segment. The 2010 Bengkulu earthquake (Fig. 4g) also caused small positive ΔCFS_m of ~0.04 MPa and ~0.02 MPa on the Dikit and Ketaun segments and negative ΔCFS_m of about -0.02 MPa on the Suliti segment.

6. Estimation Of Tectonic Stress Rate

Apart from the ΔCFS_m imparted by megathrust events, the tectonic stress rate also plays an important role in determining the Coulomb Failure Stress acting on a fault at any time. Here we denote the tectonic stress contribution to CFS on the GSF as ΔCFS_t. The higher the tectonic stress rate, the faster the fault can be brought back to its critical condition after rupture, and vice versa (Hori and Oike 1999). The tectonic stress acting on the GFS comes from two sources: (1) coupling of the oblique convergence at the megathrust, which transmits the stress acting on the megathrust through the forearc sliver and onto the GSF, and (2) arc-parallel motion of the forearc sliver itself, which exerts an additional traction on the GSF (Fitch 1972; Malod and Kemal 1996). Earlier studies (e.g., McCaffrey 2009) suggested there is a strong northward increase of the slip rate of the GSF, which would result in stretching of the forearc and imply a commensurate northward increase in tectonic stress rate. However, the more recent study of Bradley et al. (2017) uses GPS measurements of crustal velocities to show that the Sumatra forearc sliver undergoes little or no internal permanent deformation, but experiences arc-parallel movement that is consistent with an almost constant slip rate of 15 mm/yr along the GSF indicated by revised geologic estimates of the slip rate (Bradley et al. 2017; Natawidjaja et al. 2017).

We calculate ΔCFS_t for two cases: (1) tectonic stress solely due to coupling of the oblique plate convergence at the megathrust, and (2) tectonic stress due to the megathrust coupling as well as sliver movement with respect to the Sunda plate as described by Bradley et al. (2017). The former, no-sliver-movement case, is useful for comparison with other forearcs, like SW Japan, that are buttressed and have less sliver movement. The latter, sliver movement case, is preferred because it better explains the available GPS data (Bradley et al. 2017).

We derive coupling models for both cases, using the 3-block model of Bradley et al. (2017) for the transition between Indian and Australian plate motion with respect to the Sunda Plate, as illustrated in Fig. 5. For case (1) with no sliver motion, all of the oblique plate convergence between these blocks and

the Sunda plate is applied as a “back-slip” dislocation on the megathrust (Savage 1983). For case (2), the arc-parallel motion of the forearc sliver is subtracted from the oblique plate convergence in order to determine the back-slip applied on the megathrust, and then the forearc sliver movement is added to all the velocities calculated in the sliver. In both cases we have allowed coupling in the four segments: Aceh-Nias, Batu, Padang and Enggano to vary, as indicated in Fig. 5. We used a grid search over these four coupling values to find the combination resulting in the best fit to the GPS data for each of cases (1) and (2) – shown in Fig. 5a and b, respectively. We note that in both cases, similar fits to the GPS data were obtained for the Padang and Batu segments, but only case (2), with sliver movement, results in a good fit for the data in the Aceh-Nias and Enggano segments.

In order to model the elastic deformation of the forearc sliver due to coupling of the plate convergence at the megathrust, an appropriate distribution of coupling is applied along the megathrust. We use the Triangular Dislocation Element (TDE) approach of Meade (2007) to calculate the elastic deformation due to back-slip applied on triangular elements used to tesselate the irregular shape of the SLAB2.0 model (Hayes 2018) for the Sumatra megathrust (see Fig. 5). We can estimate the stress tensor using Hooke’s law, $\sigma = \lambda tr\left(\epsilon\right)\mathbf{I} + 2\mu\epsilon$, where ϵ is the strain tensor caused by the back-slip dislocation, $tr\left(\epsilon\right)$ is the trace of the strain tensor and $\mathbf{I}$ is the identity matrix. The shear stress and normal stress can then be resolved on each segment of the GSF to calculate the associated ΔCFS_t according to Equation 2. For case 1, with no sliver movement, this corresponds to the total Coulomb stress change ΔCFS_t^1 (Table 3).

Table 3

Estimation of the rates of increase in tectonic stress on the GSF for the two cases considered: (1) no forearc sliver movement and (2) forearc sliver movement from Bradley et al. (2017). In each case, $\Delta\tau$ and $\Delta\sigma$ are perturbations to shear and normal stress, respectively on each GSF segment caused by the coupling of oblique convergence at the Sumatra megathrust. For case (1), these are combined according to eq. (2) to yield ΔCFS_t^1. For case (2), an additional term $\Delta\tau_s$, calculated from the slip deficit Δu_s on each GSF segment associated with sliver movement according to Kanamori & Anderson (1975), is added to $\Delta\tau$ in order to calculate the change in Coulomb stress $\Delta CFSt^2$. θ is the angle between the forearc sliver and Sunda plate motion and at each segment.

Segment	No Sliver Movement			Sliver Movement					
	$\Delta\tau$	$\Delta\sigma$	ΔCFS_t^1	$\Delta\tau$	$\Delta\sigma$	Δu_s	$\Delta\tau_s$	θ	ΔCFS_t^2
	kPa	kPa	kPa	kPa	kPa	mm	kPa	o	kPa
Seulimeum	1.2	-3.8	0.8	0.6	-3.5	16	17.7	19	18.0
Aceh	1.0	-4.4	0.6	0.5	-4.0	15	16.7	25	16.8
Tripa North	-0.9	-4.1	-1.3	-0.9	-3.5	12	13.0	44	11.7
Tripa South	1.4	-3.9	1.0	1.1	-3.8	16	17.3	12	18.0
Renun	0.9	-4.2	0.5	0.7	-4.3	15	17.1	12	17.4
Toru	0.7	-3.2	0.3	0.5	-3.5	16	17.3	-3	17.5
Angkola	0.7	-1.9	0.5	0.5	-1.9	16	17.3	2	17.6
Barumun	0.9	-1.5	0.7	0.6	-1.6	15	16.6	-16	17.1
Sumpur	1.5	-1.9	1.4	1.6	-2.2	15	16.5	-18	17.9
Sianok	1.8	-3.5	1.4	1.9	-4.3	16	17.3	-6	18.8
Sumani	1.9	-4.2	1.5	2.0	-5.5	15	17.2	-11	18.6
Suliti	1.6	-4.7	1.1	1.3	-6.4	16	17.4	-7	18.1
Siulak	1.8	-4.9	1.3	1.4	-6.7	16	17.4	-10	18.1
Dikit	1.4	-5.0	0.9	0.7	-6.7	16	17.6	-5	17.7
Ketaun	1.0	-5.0	0.5	-0.2	-6.4	16	17.7	-6	16.8
Musi	0.9	-3.4	0.6	-0.8	-3.9	16	17.5	-12	16.3
Manna	1.2	-3.1	0.8	-0.3	-1.9	16	17.9	-4	17.4
Kumering	1.7	-3.7	1.3	0.5	-1.9	16	17.6	-12	17.9
Semangko	2.4	-3.89	2.0	0.79	-2.11	15.6	17.38	-16	18.0

As for the case (2) with sliver movement, the whole calculation is similar to what we have used for no sliver movement, however, we use the forearc rigid block movement of Bradley et al. (2017) to calculate a slip deficit for each GSF segment (Δu_s in Table 3). Then, we calculate the corresponding shear stress accumulation $\Delta\tau_s$ based on the relation of Kanamori and Anderson (1975), and add this to the shear stress $\Delta\tau$ obtained from dislocation modelling for Sumatra megathrust coupling, to obtain the total ΔCFS_t[2] for case (2) as:

$$\Delta CFS = \Delta + \Delta\tau_s + \mu' \Delta\sigma$$

3

An important caveat to this approach is its failure to account for fault-normal sliver movement, as indicated in Table 3 by the angle θ between the forearc sliver and Sunda plate motion and at each segment. Except for the Tripa North segment, this angle is generally less than 20^o, with mostly negative angles indicating extension in the south and positive angle indicating compression in the north, consistent the forearc sliver's pole location and sense of rotation (Bradley et al. 2017). The fault-normal movement must be accommodated either by oblique motion on the GSF itself, or by faulting and/or folding in the forearc sliver. Since there is little or no information on the dip of the GSF segments and internal strain rates of the sliver are not detectable using currently available GPS data (Bradley et al. 2017), we do not account for this motion here.

7. Discussion

7.1 Evaluation of ΔCFS_m imparted by Sumatran megathrust earthquakes on the GSF

We estimated the accumulation of ΔCFS_m imparted by the eight Mw > 8.0 megathrust events between 1797-2010 to the GSF (Fig. 4), and display the cumulative values of these on the different segments of the Sumatra fault in Fig. 6. The distribution of the cumulative ΔCFS_m along the GSF exhibits high positive values in the north and south, but lower and even negative values in the central part of Sumatra.

The contribution to the cumulative ΔCFS_m made by the major Sumatran megathrust events between 1797-1907 affected mainly the southern GSF, showing a cumulative ΔCFS_m of 0.1 to 0.4 MPa on the Siulak-Manna segments, and a slight increase of 0.04 MPa on the northern GSF, particularly on the Renun and Toru segments. This high ΔCFS_m in the southern part of GSF was followed by 4 major (magnitude ≥ 7) events observed from the Siulak to Manna segments between 1890-1943. During this same period, however, a similar number of major events occurred on the central and northern GSF, and also one on the Kumering segment far to the south, where ΔCFS_m did not exceed 0.04 MPa and was in some places negative. Thus, while at first glance the correlation between the pre-1907 megathrust earthquakes and

subsequent GSF earthquakes might seem high (e,g. see Fig. 2), a detailed examination of the ΔCFS_m results suggests otherwise.

The cumulative ΔCFS_m displayed in Fig. 6 also includes contributions from the four M >7.6 Sumatran megathrust earthquakes between 2004 and 2010. The distribution of ΔCFS_m imparted by these four events to the central and southern GSF is similar to that of the 1797 and 1833 earthquakes, with particularly large ΔCFS_m on the Musi and Manna segments. The main difference in the ΔCFS_m distribution for the 21st century megathrust events with that of the pre-1907 events is the contribution of the 2004 Sumatra-Andaman earthquake, resulting in an increase of nearly 0.3-0.5 MPa on the Seulimeum-Aceh segment. The 2007 Bengkulu earthquake resulted in positive ΔCFS_ms of 0.9 and 0.8 MPa on the Manna and Musi segments, respectively, remarkably similar to the pattern following the 1833 Bengkulu earthquake. None of the 21st century Sumatra megathrust events have been followed by major GSF events, with the exception of the magnitude 6.6 earthquake in the Dikit segment, despite the expectation following the 2004 Sumatra-Andaman earthquake that a major GSF earthquake was imminent (McCloskey et al. 2005).

The values of ΔCFS_m that we obtain for the northern GSF due to the 2004 and 2005 megathrust earthquakes are less than those of McCloskey et al. (2005) and Qiu and Chan (2019), who obtained maximum ΔCFS_m of 0.9 MPa and 1.5 MPa, respectively. This is most likely due to a combination of two factors. First, our reported ΔCFS_m of 0.4MPa is the average for the Seulimeum-Aceh segment, which actually experiences a maximum ΔCFS of 0.7 MPa. Second, Qiu and Chan (2019) assumed a high effective friction values of $\mu' = 0.4$, while we used $\mu' = 0.1$(McCloskey et al. 2005, do not say what value they used). As explained above, we prefer the low value μ'=0.1 along the GSF because it agrees with studies of the SW Japan forearc and of large, crustal strike-slip faults (Carpenter et al. 2015; Iio 1997; Hori and Oike 1999; Mitogawa and Nishimura 2020; Shikakura et al. 2014; Provost et al. 2003; Townend and Zoback 2006).

7.2 Stress Changes Time Evolution on the GSF Without Sliver Movement

In order to model the time evolution stress changes on any GSF segment, we need the results of ΔCFS_m due to megathrust earthquakes, the tectonic stress rate ΔCFS_t, and the stress drops of large intraplate earthquakes on nearby GSF segments. Table 1 shows the slip of each GSF earthquake calculated using the relationship between magnitude and Average Displacement (AD) of Wells and Coppersmith (1994) based on a linear regression of global magnitude and slip data. We also used the relation of Kanamori and Anderson (1975) to calculate stress drops of all large (M ≥ 6.5) GSF earthquakes, assuming down-dip rupture width of 20 km. We note that several earthquakes are unlikely to have involved full segment rupture and may not have ruptured the full downdip width, so the stress drops in Table 1 may be underestimated for these events. We used the Wells and Coppersmith (1994) formula for rupture area vs. magnitude to estimate the fraction of the full segment area that ruptured. If we consider 7 events that

ruptured more than 50% of the segment area to have ruptured the full downdip width, and find that these earthquakes have stress drops of 1.8-3.4 MPa, which we adopt as characteristic for the GSF. For the effects that GSF earthquakes have on adjacent GSF segments, we assume that only these seven earthquakes are significant, and have neglected the contribution of smaller earthquakes. With these results as well as those of previous sections, we can model the time evolution of CFS changes on the GSF from 1750 to 2050 (see Fig. 7).

As shown in Table 3, the estimated increase in tectonic stress rates on the GSF with the case (1) of no sliver movement produces a tectonic stress rate of 0.5-2.0 KPa/yr. This low rate of tectonic stress increase is similar to that obtained by Shikakura et al. (2014) and Mitogawa and Nishimura (2020) for SW Japan's Nankai Trough forearc. If we consider 1.8-3.4 MPa as the threshold level for earthquakes to occur, this would imply a recurrence interval of 1000-700 years, not dissimilar to the 1000-3000 suggest by paleoseismic studies of SW Japan's MTL (Tatsumi and Okada 1996). On the other hand, the characteristic slip of the 7 full-with earthquake ruptures from Table is 1.5-3.3 m, and the recently revised (Bradley et al. 2017) slip rate for the GSF is about 15 mm/yr. Estimating a recurrence interval using a slip-predictable model (Shimazaki and Nakata 1980) would suggest a much shorter recurrence time of 100-220 years, about an order of magnitude shorter than suggested by the low tectonic stress rate of case (1), with no sliver movement.

A low tectonic stress rate implies a recurrence time of 1000 years or more for GSF earthquakes, much longer than the recurrence time of 130-450 years of major Sumatra megathrust earthquakes (Malik et al. 2019; Philibosian et al. 2014; Rubin et al. 2017). Given that the ΔCFS_m such an earthquake imparts to the GSF can be as much as 1 MPa, and the typical stress drops of large GSF earthquakes can be 1.8-3.4 MPa, large Sumatra megathrust earthquakes should be able to bring forward fault failure times on the GSF by hundreds of years. For example, the Musi and Manna segments experience tectonic stress rates of 0.6 and 0.8 kPa/year, and the 1833 megathrust earthquake resulted in ΔCFS_ms of 0.4 and 0.2 MPa, respectively. If the GSF earthquakes in this segment followed a stress-predictable mode, their rupture times would have been brought forward by 650 years for Musi and 250 years for Manna. Since earthquakes did in fact occur only 60-70 years after the 1833 event, it would be logical to conclude that their occurrence was significantly influenced by the megathrust earthquake. Furthermore, while the low tectonic stress rate might lead one to expect it would take over 1000 years for stress to accumulate to the level required for earthquake recurrence, the 2007 Sumatra megathrust earthquake has moved these forward so that the Musi and Mannai segments could rupture in a large earthquake even now.

On the other hand, despite the fact that the 2004 Sumatra-Andaman earthquake was widely regarded as having the potential to trigger a large GSF earthquake on the Seulimeum segment (McClosky et al. 2005), Fig. 7a suggests that, although the 2004/2005 earthquakes may have brought forward rupture there by 375 years, the ΔCFS_m was not large enough to bring the CFS to the same level at which the segment ruptured in 1964. Case (1) nevertheless suggests that large megathrust earthquakes on the Sumatra fault can bring forward rupture of GSF earthquakes by hundreds of years, and in that sense, they could have a strong influence on the time-dependent seismic hazard in the Sumatra forearc.

7.3 Time Evolution of Coulomb Stress Changes on the GSF with Forearc Sliver Movement

For the case (2) of including forearc sliver movement (Fig. 7b), the tectonic stress rate is 14-15 times greater than in case (1). This rate is much higher than in SW Japan, and this is almost certainly the reason that the GSF has a much higher level of earthquake activity than the MTL. In fact, for case (2) the tectonic stress rate is so high that the ΔCFSs due to both megathrust earthquakes and GSF earthquakes in adjacent segments, are much less significant. The time evolution of the Coulomb stress on any segment of the GSF is essentially controlled by the high tectonic stress rate and occurrence of large earthquakes on that segment. If we consider that the range of stress drops for full-width rupture of past GSF earthquakes (Table 1) is 1.8-3.4 MPa, and that the average tectonic stress rate is 17 kPa/year, it takes 100-200 years for the CFS to recover its pre-earthquake level following a major event. A similar conclusion could be drawn from a consideration of the characteristics slip of 1.8-3.3 m and the ≈ 15-16 mm/yr slip rate determined from geodetic and geologic data (Bradley et al. 2017; Ito et al. 2012; Natawidjaja et al. 2017; Natawidjaja 2018a, b).

For this case, all segments on the northern part of the GSF have experienced large increases in CFS throughout the interval studied, and segments that have had large earthquakes in the past – the Seulimeum, Tripa North and South, Renun and Angkola segments – have already seen CFS recover to what it was prior to the respective earthquake. In the southern part of the GSF, the Sumani and Suliti segments appear to have not yet recover from the previous large GSF earthquake. The Siulak segment on the other hand, despite experience decreases in CFS following the occurrence of a small GSF earthquake in 1995 and the 2007 megathrust earthquakes, has almost recovered from the large decrease in CFS it experienced during a large (Ms 7.3) earthquake in 1909. The Ketaun segment is similarly close to having recovered from a major earthquake it experienced in 1943, while the Kumering segment has yet to recover from the CFS decrease it experienced during a major earthquake in 1933.

Of considerable concern in Fig. 7b are the GSF segments that have never experienced a major earthquake since the high tectonic stress rate results in an increase of CFS on these segments of 5-6 MPa. These include the Aceh, Toru, Barumun, Sumpur, Sianok, and Semangko segments. First, it should be noted that the history of large GSF earthquakes is complete only since 1892 (Hurukawa et al., 2014), so any of these segments could have experienced a large earthquake at almost any time during the 19th century that could have substantially reduced its accumulated CFS over the 1750-2050 period. Second, some of these segments may be creeping. GPS (Ito et al. 2012) and Interferometric Synthetic Aperture radar (Tong et al. 2018) have confirmed that the Aceh segment is creeping, but geodetic studies on other segments have resolution that is too poor to establish whether they are creeping or not.

Whether we consider forearc sliver movement or not, the Musi and Manna segments appear to have accumulated enough stress that CFS has recovered to the level it was at prior to large earthquakes on these segments.

8. Conclusion

We have estimated and investigated the effect of the historical accumulation of Coulomb stress on the GSF from the late 16th to early 21st centuries, spanning the occurrence eight great Sumatra megathrust earthquakes (1797 to 2010 earthquakes). This involved the estimation of the tectonic stress rate on the GSF, for which we have considered two cases: (1) no arc-parallel movement of the forearc sliver, to better compare with buttressed forearcs in other obliquely convergent margins, and (2) including the relatively fast (15-17 mm/yr) arc-parallel movement of the forearc sliver that is consistent with recent GPS studies of the Sumatra forearc (Bradley et al., 2017).

For the case with no arc-parallel movement of the forearc sliver, the tectonic stress rate on the GSF (denoted ΔCFS^1 in Table 3) is determined solely by the coupling of obliquely convergent plate motion at the megathrust. In this case, the tectonic stress rate is very low, with all but the Tripa North segment experiencing a rate of between 0.3-2.0 kPa (the stress rate on the Tripa North segment is negative for this case, probably due to accommodation of thrust movement that was not considered here). This suggests a recurrence interval for full segment rupture of 1000 years or greater. Both the low tectonic stress rate and long earthquake recurrence interval are similar to those obtained for SW Japan's Nankai Trough (Hori and Oike 1996; Mitogawa and Nishimura 2020; Shikakura et al. 2014) and are likely typical of other forearcs whose arc-parallel motion is impeded by a buttressed leading edge (Beck et al. 1993). This case appears to have an order of magnitude less earthquake activity than is observed on the GSF, and the forearc deformation does not match GPS measurements of crustal velocity in the northern and southern parts of the Sumatra forearc sliver. In this case, co-seismic changes in CFS can advance rupture by hundreds of years, so in that sense modulation of GSF earthquakes by megathrust events is important.

For the case including 15-17 mm/yr of arc-parallel sliver movement, which Bradley et al. (2017) show match the GPS data well throughout the length of the Sumatra forearc, the tectonic stress rate (ΔCFS^2 in Table 3) is 9 to 58 times higher than when there is no sliver movement. The recurrence interval for full-segment rupture is 100-200 years, roughly consistent with a slip-predicable model in which such ruptures experience 1.5-3.3 m slip (Table 1) at the observed slip rate of 15-16 mm/yr (Bradley et al. 2017). In this case, changes in CFS imparted by megathrust earthquakes advance rupture by only a few years, and in this sense, they are not very important, though they may still modulate GSF event occurrence to some extent. In summary, seismic hazard along the great Sumatra fault is driven much more by the rapid arc-parallel forearc sliver motion than by megathrust earthquake activity. The Sumatra forearc may be unique in this respect, since instead of being buttressed at its leading edge, arc-parallel motion of the sliver appears to be accommodated by seafloor spreading in the Andaman Sea to the north of Sumatra (Curray 2005).

A concern highlighted in this study is the potentially high stress accumulation on the GSF segments that have never experienced full segment rupture, like the Aceh, Toru, Barumun, Sumpur, Sianok, and Semangko segments. Although the Aceh segment is creeping (Tong et al, 2018; Ito et al., 2012) and therefore unlikely to accumulate the high level of stress indicated in Fig. 7b, it is unknown whether the

other segments are creeping or not. It is entirely possible that some of these segments may have ruptured in the early to mid-19th century, when historical records are sparse, which would reduce the accumulated stress. A new compilation of historical data by Martin et al. (2018) suggest some of these segments are likely to have ruptured early in the 19th century, although the magnitudes are difficult to constrain. In any case, further study of creep on these segments would help constrain seismic hazard along the GSF. On the other hand, some segments that have experienced full-segment rupture and are therefore likely locked, such as the Tripa (North and South), Angkola, Musi and Manna segments appear to be well advanced in their seismic cycles and could experience another large event soon.

Finally, we point out that our model of the GSF is simplified, and likely does not account for much of the complexity on the actual GSF. Segment geometries have been simplified and are all assumed to be pure strike-slip, when in reality some segments likely involve some component of oblique motion. Although Bradley et al. (2017) find that the available GPS data are best fit with no internal deformation of the Sumatra forearc sliver, there may be some deformation that is simply not resolved by the relatively sparse station spacing, and such internal deformation would likely reduce the tectonic stress rates calculated in Table 3. Nevertheless, we believe the model we have developed in this study for stress accumulation and release along the GSF will prove useful in guiding further seismic hazard studies in Sumatra.

Declarations

Acknowledgment

The authors would like to thank to Directorate General of Resources for Science, Technology, and Higher Education of KEMRISTEKDIKTI for supporting this research through Program Magister menuju Doktor untuk Sarjana Unggul (PMDSU) scheme which has given to SW. Some figures in this manuscript were plotted using Global Mapping Tools (GMT) (Wessel et al. 2019) and Python.

Disclosure of potential conflicts of interest

The author declare that the research was conducted in the absence of any commercial and financial relationships that could be construed as a potential conflict of interest.

Studies involving animal subjects

No animal studies are presented in this manuscript.

Studies involving human subjects

No human studies are presented in this manuscript.

Statement of Informed Consent

There are no human subjects in this article and informed consent is not applicable.

Funding

This research was supported by the Directorate General of Resources for Science, Technology, and Higher Education of the Ministry of Research, Technology, and Higher Education (KEMRISTEKDIKTI) of Republic of Indonesia through Program Magister menuju Doktor untuk Sarjana Unggul (PMDSU) scheme which has given to SW.

Competing Interests

The authors have no relevant financial or non-financial interests to disclose.

Author Contributions

All authors contributed to the study conception and design. Muhammad Taufiq Rafie contributed to the stress estimation of megathrust and Sumatran fault earthquakes. Phil R. Cummins contributed to the coupling and tectonic stress rate estimation. Muhammad Taufiq Rafie, David P. Sahara, Phil R. Cummins, Wahyu Triyoso, and Sri Widiyantoro contributed to the analysis of the results. David P. Sahara, Phil R. Cummins, Wahyu Triyoso, and Sri Widiyantoro contributed to supervise and validate the results. All authors contributed to the preparation of the manuscript. All authors read and approved the final manuscript.

Data Transparency

The original contributions presented in the study are included in the article/supplementary material, further inquiries can be directed to the corresponding author/s.

References

1. Ammon CJ, Ji C, Thio H, Robinson D, Ni S, Hjorleifsdottir V, Kanamori H, Lay T, Das S, Helmberger D, Ichinose G, Polet J, Wald D (2005) Rupture process of the 2004 Sumatra-Andaman earthquake. Science 308:1133-1139. http://doi.org/10.1126/science.1112260
2. Beck ME (1991) Coastwise transport reconsidered: lateral displacements in oblique subduction zones, and tectonic consequences. Physics of the Earth and Planetary Interiors 68:1-8. https://doi.org/10.1016/0031-9201(91)90002-Y
3. Beck ME, Rojas C, Cembrano J (1993) On the nature of buttressing in margin-parallel strike-slip fault systems. Geology 21:755–758. https://doi.org/10.1130/0091-7613(1993)021<0755:OTNOBI>2.3.CO;2
4. Bradley KE, Feng L, Hill EM, Natawidjaja DH, Sieh K (2017) Implications of the diffuse deformation of the Indian Ocean lithosphere for slip partitioning of oblique plate convergence in Sumatra. Journal of Geophysical Research: Solid Earth 122:572-591. Doi: 10.1002/2016JB013549
5. Briggs R, Sieh K, Meltzner A, Natawidjaja D, Galetzka J, Suwargadi B, Hsu Y, Simons M, Hananto N, Suprihanto I (2006) Deformation and slip along the Sunda megathrust in the great 2005 Nias-

Simeulue earthquake. Science 311(5769):1897-1901. http://doi.org/10.1126/science.1122602

6. Carpenter BM, Saffer DM, Marone C (2015) Frictional properties of the active San Andreas Fault at SAFOD: Implications for fault strength and slip behavior. Journal of Geophysical Research: Solid Earth 120(7): 5273–5289. http://doi.org/10.1002/2015JB011963
7. Cattin R, Chamot-Rooke N, Pubellier M, Rabaute A, Delescluse M, Vigny C, Fleitout L, Dubernet P (2009). Stress changes and effective friction coefficient along the Sumatra-Andaman-Sagaing fault system after the 26 December 2004 (Mw= 9.2) and the 28 March 2005 (Mw= 8.7) earthquakes. Geochemistry, Geophysics, Geosystem 10(3). https://doi.org/10.1029/2008GC002167
8. Curray JR (2005) Tectonics and history of the Andaman Sea region. Journal of Asian Earth Sciences 25(1):187–232. https://doi.org/10.1016/j.jseaes.2004.09.001
9. Di Giacomo D, Engdahl ER, Storchak DA (2018). The ISC-GEM Earthquake Catalogue (1904-2014): status after the Extension Project. Earth System Science Data 10:1877-1899. Doi: 10.5194/essd-10-1877-2018
10. Fitch TJ (1972) Plate convergence, transcurrent faults, and internal deformation adjacent to southeast Asia and the western Pacific. Journal of Geophysical Research 77(23):4432-4460. https://doi.org/10.1029/JB077i023p04432
11. Genrich JF, Bock Y, McCaffrey R, Prawirodirdjo L, Steven CW, Puntodewo SSO, Subarya C, Wdowinski S (2000) Distribution of slip at the northern Sumatran fault system. Journal of Geophysical Research: Solid Earth 105(B12):28327-28341. https://doi.org/10.1029/2000JB900158
12. Harris RA (1998) Introduction to special section – Stress triggers, stress shadows, and implication for seismic hazard. Journal of Geophysical Research 103:24347-24358. https://doi.org/10.1029/98JB01576
13. Hayes GP (2017) The finite, kinematics rupture properties of great-sized earthquake since 1990. Earth and Planetary Science Letters 468:94-100. https://doi.org/10.1016/j.epsl.2017.04.003
14. Hayes GP (2018) Slab2 – A comprehensive subduction zone geometry model. U.S. Geological Survey data release. https://doi.org/10.5066/F7PV6JNV
15. Hori T, Oike K (1999) A physical mechanism for temporal variation in seismicity in Southwest Japan related to the great interplate earthquakes along the Nankai trough. Tectonophysics 308(1-2):83-98. https://doi.org/10.1016/S0040-1951(99)00079-7
16. Hurukawa N, Wulandari BR, Kasahara M (2014) Earthquake history of the Sumatran fault, Indonesia, since 1892, derived from relocation of large earthquakes. Bulletin of the Seismological Society of America 104(4): 1750-1762. https://doi.org/10.1785/0120130201
17. Irsyam M, Cummins PR, Asrurifak M, Faizal L, Natawidjaja DH, Widiyantoro S, Meilano I, Triyoso W, Rudiyanto A, Hidayati S, Ridwan M, Hanifa NR, Syahbana AJ (2020) Development of the 2017 national seismic hazard maps of Indonesia. Earthquake Spectra. http://doi.org/10.1177/8755293020951206
18. Iio Y (1997) Frictional coefficient on faults in a seismogenic region inferred from earthquake mechanism solutions. Journal of Geophysical Research: Solid Earth 102(B3):5403-5412.

https://doi.org/10.1029/96JB03593

19. Ito T, Gunawan E, Kimata F, Tabei T, Simons M, Meilano I, Agustan, Ohta Y, Nurdin I, Sugiyanto D (2012) Isolating along-strike variations in the depth extent of shallow creep and fault locking on the northern Great Sumatran Fault. Journal of Geophysical Research 117(B6). https://doi.org/10.1029/2011JB008940
20. Jarrad RD (1986) Terrane motion by strike-slip faulting of forearc slivers. Geology 14:780–783. https://doi.org/10.1130/0091-7613(1986)14<780:TMBSFO>2.0.CO;2
21. Kanamori H, Anderson DL (1975) Theoretical basis of some empirical relations in seismology. Bulletin of the Seismological society of America 65(5):1073-1095. https://doi.org/10.1785/BSSA0650051073
22. Kapoor DC (1981) General bathymetric chart of the oceans (GEBCO). Marine Geodesy 5(1):73-80. https://doi.org/10.1080/15210608109379408
23. Kimura G (1986) Oblique subduction and collision: forearc tectonics of the Kuril arc. Geology 14(5):404–407. https://https://doi.org/10.1130/0091-7613(1986)14<404:OSACFT.2.0.CO;2
24. King GCP, Stein RS, Lin J (1994) Static stress changes and the triggering of earthquakes. Bulletin of the Seismological Society of America 84(3):935-953. https://doi.org/10.1785/BSSA0840030935
25. Konca AO, Hjorleifsdottir V, Song TA, Avouac J, Helmberger DV, Ji C, Sieh K, Briggs R, Meltzner A (2007) Rupture kinematics of the 2005, Mw 8.6, Nias-Simeulue from the joint inversion of seismic and geodetic data. Bulletin of the Seismological Society of America 97(1A):307-322. https://doi.org/10.1785/0120050632
26. Konca AO, Avouac JP, Sladen A, Meltzner AJ, Sieh K, Fang P, Li Z, Galetzka J, Chlieh M, Natawidjaja DH (2008) Partial rupture of a locked patch of the Sumatra megathrust during the 2007 earthquake sequence. Nature 456(7222):631-635. https://doi.org/10.1038/nature07572
27. Kreemer C, Blewitt G, Klein EC (2014) A geodetic plate motion and Global Strain Rate Model. Geochemistry Geophysics Geosystems 15(10):3849–3889. https://doi.org/10.1002/2014GC005407
28. Lin J, Stein RS (2004) Stress triggering in thrust and subduction earthquakes and stress interaction between the southern San Andreas and nearby thrust and strike-slip faults. Journal of Geophysical Research: Solid Earth 109(B2). https://doi.org/10.1029/2003JB002607
29. Mai PM, Thingbaijam KKS (2014) SRCMOD: An online database of finite-fault rupture models. Seismological Research Letters 85(6):1348-1357. https://doi.org/10.1785/0220140077
30. Malik JN, Johnson FC, Khan A, Sahoo S, Irshad R, Paul D, Arora S, Baghel PK, Chopra S (2019) Tsunami records of the last 8000 years in the Andaman Island, India, from mega and large earthquakes: Insights on recurrence interval. Scientific Reports 9(18463). http://doi.org/10.1038/s41598-019-54750-6
31. Malod JA, Kemal BM (1996) The Sumatra margin: oblique subduction and lateral displacement of the accretionary prism. Geological Society, London, Special Publication, 106(1):19-28. https://doi.org/10.1144/GSL.SP.1996.106.01.03

32. Martin SS, Locati M, Sieh K (2018) Gempa Nusantara: a new digital database of felt intensity for historical earthquakes in the Indonesian archipelago. In *2018 Seismology of the Americas Meeting*. Seismological Society of America.
33. Martin SS, Li L, Okal EA, Morin J, Tetteroo AE, Switzer AD, Sieh KE (2019) Reassessment of the 1907 Sumatra “tsunami earthquake” based on macroseismic, seismological, and tsunami observations, and modeling. Pure and Applied Geophysics 176(7):2831-2868. https://doi.org/10.1007/s00024-019-02134-2
34. McCaffrey R (1991) Slip vectors and stretching of the Sumatran fore arc. Geology 19(9):881-884. https://doi.org/10.1130/0091-7613(1991)019<0881:SVASOT>2.3.CO;2
35. McCaffrey R (1992) Oblique plate convergence, slip vectors, and forarc deformation. Journal of Geophysical Research: Solid Earth 97:8905-8915. https://doi.org/10.1029/92JB00483
36. McCaffrey R (2009) The tectonic framework of the Sumatran subduction zone. Annual Review of Earth and Planetary Sciences 3737:345-366. https://doi.org/10.1146/annurev.earth.031208.100212
37. McCloskey J, Nalbant S, Steacy S (2005) Earthquake risk from co-seismic stress. Nature 434:291. https://doi.org/10.1038/434291a
38. Meade BJ (2007) Algorithm for the calculation of exact displacements, strains, and stresses for triangular dislocation elements in a uniform elastic half space. Computers & geosciences 33(8):1064-1075. https://doi.org/10.1016/j.cageo.2006.12.003
39. Meltzner AJ, Sieh K, Chiang HW, Wu CC, Tsang LL, Shen CC, Hill EM, Suwargadi BW, Natawidjaja DH, Philibosian B, Briggs RW (2015) Time-varying interseismic strain rates and similar seismic ruptures on the Nias-Simeulue patch of the Sunda megathrust. Quaternary Science Reviews 122:258-281. https://doi.org/10.1016/j.quascirev.2015.06.003
40. Mildon ZK, Toda S, Faure Walker JP, Roberts GP (2016) Evaluating models of Coulomb stress transfer: Is variable fault geometry important?. Geophysical Research Letters 43(24):12407-12414. https://doi.org/10.1002/2016GL071128
41. Mildon ZK, Roberts GP, Walker JF, Toda S (2019) Coulomb pre-stress and fault bends are ignored yet vital factors for earthquake triggering and hazard. Nature Communication 10(1):1-9. https://doi.org/10.1038/s41467-019-10520-6
42. Mitogawa T, Nishimura T (2020) Coulomb stress changes on inland faults during megathrust earthquake cycle in southwest Japan. Earth, Planets and Space 72. https://doi.org/10.1186/s40623-020-01174-6
43. Natawidjaja DH, Sieh K, Chlieh M, Galetzka J, Suwargadi BW, Cheng H, Edwards RL, Avouac JP, Ward SN (2006) Source parameters of the great Sumatran megathrust earthquakes of 1797 and 1833 inferred from coral microatolls. Journal of Geophysical Research: Solid Earth 111(B6). https://doi.org/10.1029/2005JN004025
44. Natawidjaja DH, Triyoso W (2007) The Sumatran fault zone – From source to hazard. Journal of Earthquake and Tsunami 1(01):21-47. https://doi.org/10.1142/S1793431107000031

45. Natawidjaja DH, Bradley K, Daryono MR, Aribowo S, Herrin J (2017) Late Quaternary eruption of the Ranau Caldera and new geological slip rates of the Sumatran Fault Zone in Southern Sumatra, Indonesia. Geoscience Letters 4(1):1-15. https://doi.org/10.1186/s40562-017-0087-2
46. Natawidjaja DH (2018a) Major bifurcations, slip rates, and a creeping segment of Sumatran Fault Zone in Tarutung-Sarulla-Sipirok-Padangsidempuan, Central Sumatra, Indonesia. Indonesian Journal of Geoscience 5(2):137-160. Doi: 10.17014/ijog.5.2.137-160
47. Natawidjaja DH (2018b) Updating active fault maps and slip rates along the Sumatran Fault Zone, Indonesia. IOP Conference Series: Earth and Environmental Science 188. Doi: 10.1088/1755-1315/118/1/012001
48. National Center for Earthquake Studies of Indonesia (PUSGEN) (2017) Indonesia's earthquake source and hazard map (in Bahasa Indonesia). Research and Development Agency of Ministry of Public Work and Housing, Indonesia. ISBN 978-602-5489-01-3
49. Newcomb KR, McCann WR (1987) Seismic history and seismotectonics of the Sunda Arc. Journal of Geophysical Research: Solid Earth 92(B1):421-439. https://doi.org/10.1029/JB092iB01p00421
50. Okada Y (1985) Surface deformation due to shear and tensile faults in a half-space. Bulletin of the Seismological Society of America 75(4):1135-1154
51. Okada Y (1992) Internal deformation due to shear and tensile faults in a half-space. Bulletin of the Seismological Society of America 82(2):1018-1040
52. Philibosian B, Sieh K, Avouac J-P, Natawidjaja DH, Chiang H-W, Wu C-C, Perfettini H, Shen C-C, Daryono, MR, Suwargadi BW (2014) Rupture and variable coupling behavior of the Mentawai segment of the Sunda megathrust during the supercycle culmination of 1797 to 1833. Journal of Geophysical Research-Solid Earth 119(9):7258–7287. http://doi.org/10.1002/2014JB011200
53. Provost AS, Chéry J, Hassani R (2003) 3D mechanical modeling of the GPS velocity field along the North Anatolian fault. Earth and Planetary Science Letters 209:361–377. http://doi.org/10.1016/S0012-821X(03)00099-2
54. Qiu Q, Chan CH (2019) Coulomb stress perturbation after great earthquakes in the Sumatran subduction zone: Potential impacts in the surrounding region. Journal of Asian Earth Sciences 180:103869. https://doi.org/10.1016/j.jseaes.2019.103869
55. Rafie MT, Cummins PR, Sahara DP, Widiyantoro S, Triyoso W and Nugraha AD (2021) Variations in Forearc Stress and Changes in Principle Stress Orientations Caused by the 2004–2005 Megathrust Earthquakes in Sumatra, Indonesia. Frontiers in Earth Science. https://doi.org/10.3389/feart.2021.712144
56. Rhie J, Dreger D, Bürgmann R, Romanowicz B (2007) Slip of the 2004 Sumatra-Andaman earthquake from joint inversion of long-period global seismic waveforms and GPS static offsets. Bulletin of the Seismological Society of America 97:S115-S127. https://doi.org/10.1785/0120050620
57. Rivera L, Sieh K, Helmberger D, Natawidjaja DH (2002) A comparative study of the Sumatran subduction-zone earthquakes of 1935 and 1984. Bulletin of the Seismological Society of America 92:1721-1736. https://doi.org/10.1785/0120010106

58. Rubin CM, Horton B, Sieh K, Pilarczyk JE, Daley P, Ismael N, Parnell AC (2017) Highly variable recurrence of tsunamis in the 7,400 years before the 2004 Indian Ocean tsunami. Nature Communications 8(1):1–12. https://doi.org/10.1038/ncomms16019
59. Ryder I, Rietbrock A, Kelson K, Bürgmann R, Floyd M, Socquet A, Vigny C, Carrizo D (2012) Large extensional aftershocks in the continental forearc triggered by the 2010 Maule earthquake, Chile. Geophysical Journal International 188:879–890. https://doi.org/10.1111/j.1365-246X.2011.05321.x
60. Savage JC (1983) A dislocation model of strain accumulation and release at a subduction zone. Journal of Geophysical Research: Solid Earth 88(6):4984–4996. https://doi.org/10.102JB088iB06p04984
61. Sevilgen V, Stein RS, Pollitz FF (2012) Stress imparted by the great 2004 Sumatra earthquake shut down transforms and activated rifts up to 400 km away in the Andaman Sea. Proceedings of the National Academy of Sciences 109(38):15152-15156. http://doi.org/10.1073/pnas.1208799109
62. Shikakura Y, Fukahata Y, Hirahara K (2014) Long-term changes in the Coulomb failure function on inland active faults in southwest Japan due to east-west compression and interplate earthquakes. Journal of Geophysical Research: Solid Earth 119(1):502-518. https://doi.org/10.1002/2013JB010156
63. Shimazaki K, Nakata T (1980) Time-predictable recurrence model for large earthquakes. Geophysical Research Letters 7(4):279-282. https://doi.org/10.1029/GL007i004p00279
64. Sieh K, Natawidjaja DH (2000) Neotectonics of the Sumatra fault, Indonesia. Journal of Geophysical Research: Solid Earth 105(B12):28295-28326. https://doi.org/10.1029/2000JB900120
65. Stein RS (1999) The role of stress transfer in earthquake occurrence. Nature 402(6762):605-609. https://doi.org/10.1038/45144.
66. Stirling, MW, Wesnousky SG, Shimazaki K (1996) Fault trace complexity, cumulative slip, and the shape of the magnitude-frequency distribution for strike-slip faults: A global survey. Geophysical Journal International 124(3):833–868. https://doi.org/10.1111/j.1365-246X.1996.tb05641.x
67. Storchak DA, Di Giacomo D, Engdahl ER, Harris J, Bondar I, Lee WH, Bormann P, Villasenor A (2015) The ISC-GEM global instrumental earthquake catalogue (1900-2009): introduction. Physics of the Earth and Planetary Interiors 239:48-63. Doi: 10.1016/j.pepi.2014.06.009
68. Tabei T, Hashimoto M, Miyazaki S, Ohta Y (2003) Present-day deformation across the southwest Japan arc: Oblique subduction of the Philippine Sea plate and lateral slip of the Nankai forearc. Earth, Planets and Space 55:643–647. https://doi.org/10.1186/BF03352471
69. ten Brink U, Lin J (2004) Stress interaction between subduction earthquakes and forearc strike-slip faults: Modeling and application to the northern Caribbean plate boundary. Journal of Geophysical Research: Solid Earth 109(B12). https://doi.org/10.1029/2004JB003031
70. Toda S, Stein RS, Reasenberg PA, Dieterich JH, Yoshida A (1998) Stress transferred by the 1995 Mw= 6.9 Kobe, Japan, shock: Effect on aftershocks and future earthquake probabilities. Journal of Geophysical Research: Solid Earth 103(B10):24543-24565. https://doi.org/10.1029/98JB00765

71. Toda S, Stein RS, Richards-Dinger K, Bozkurt SB (2005) Forecasting the evolution of seismicity in southern California: Animations built on earthquake stress transfer. Journal of Geophysical Research: Solid Earth 110(B5). https://doi.org/10.1029/2004JB003415
72. Tong X, Sandwell DT, Schmidt DA (2018) Surface creep rate and moment accumulation rate along the Aceh segment of the Sumatran fault from L-band ALOS-1/PALSAR-1 observations. Geophysical Research Letters. 45(8):3404-3412. doi:10.1002/2017GL076723
73. Townend J, Zoback M (2004) Regional tectonic stress near the San Andreas fault in central and southern California. Geophysical Research Letters 31(15). https://doi.org/10.1029/2003GL018918
74. Tsutsumi H, Okada A (1996) Segmentation and Holocene surface faulting on the Median Tectonic Line, southwest Japan. Journal of Geophysical Research 101(B3):5855–5871. https://doi.org/10.1029/95JB01913
75. Wang K (1996) Simplified analysis of horizontal stresses in a buttressed forearc sliver at an oblique subduction zone. Geophysical Research Letters 23(16):2021–2024. https://doi.org/10.1029/96GL02067
76. Wang K (2000) Stress-strain “paradox,” plate coupling, and forearc seismicity at the Cascadia and Nankai subduction zones. Tectonophysics 319(4):321–338. https://doi.org/10.1016/S0040-1951(99)00301-7
77. Wells DL, Coppersmith KJ (1994) New empirical relationships among magnitude, rupture length, rupture width, rupture area, and surface displacement. Bulletin of the Seismological society of America 84:974-1002. https://doi.org/10.1785/BSSA0840040974
78. Wiseman K, Bürgmann R (2012) Stress triggering of the great Indian Ocean strike-slip earthquakes in a diffuse plate boundary zone. Geophysical Research Letters 39:L22304. https://doi.org/10.1029/2012GL053954.
79. Wessel P, Luis JF, Uieda L, Scharroo R, Wobbe F, Smith WHF, Tian D (2019) The Generic Mapping Tools version 6. Geochemistry, Geophysics, Geosystems 20:5556-5564. doi: 10.1029/2019/GC008515
80. Yue H, Lay T, Rivera L, Bai Y, Yamazaki Y, Cheung KF, Hill EM, Sieh K, Kongko W, Muhari A (2014) Rupture process of the 2010 Mw 7.8 Mentawai tsunami earthquake from joint inversion of near-field hr-GPS and teleseismic body wave recordings constrained by tsunami observations. Journal of Geophysical Research: Solid Earth 119(7):5574-5593. https://doi.org/10.1002/2014JB011082

Figures

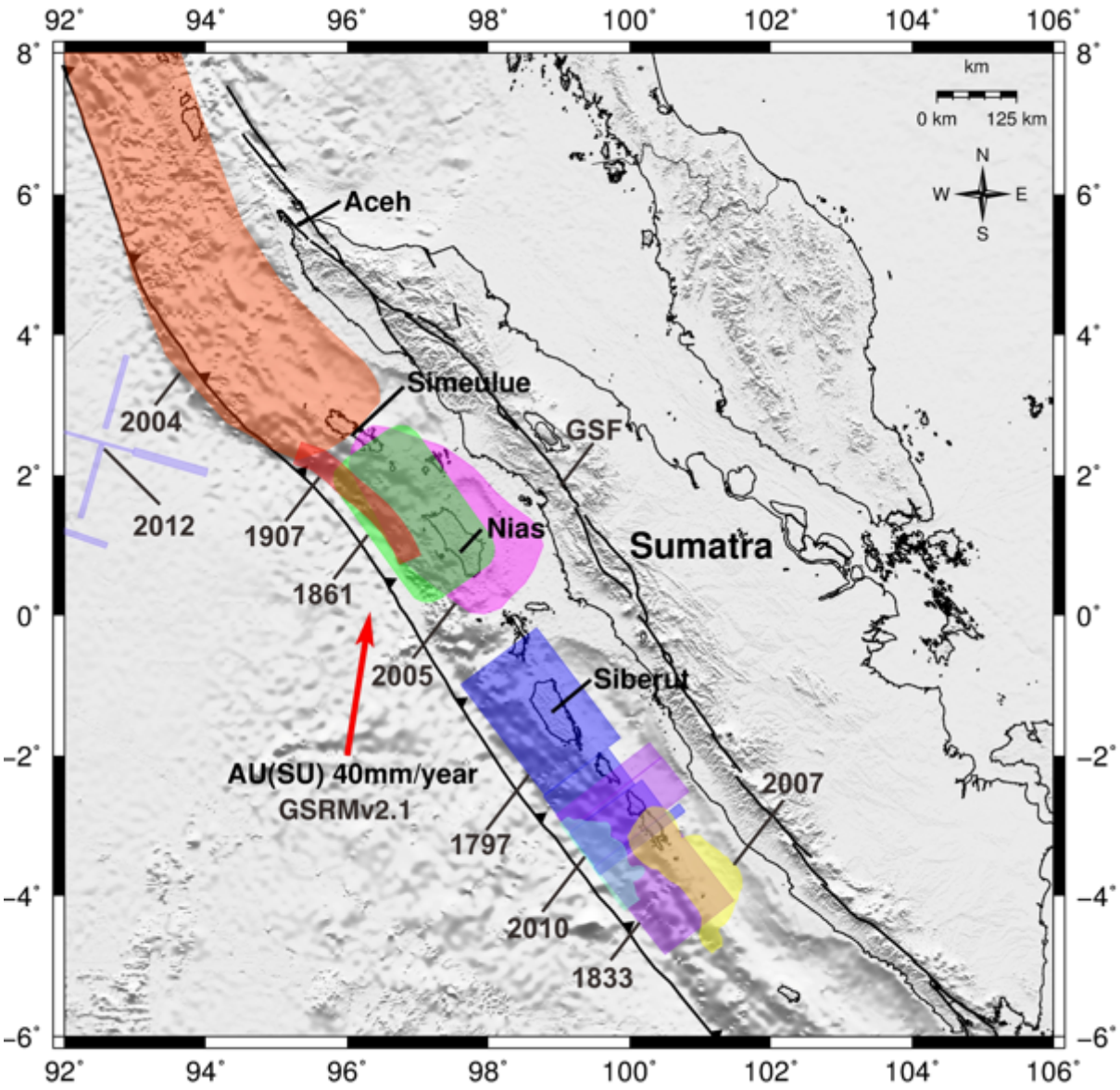

Figure 1

Historical ruptures of the Sunda megathrust earthquake between 1797 to 2012 compiled from previous studies Natawidjaja et al. (2006), Rivera et al. (2002), Martin et al. (2019), Rhie et al. (2007), Konca et al. (2007), Konca et al. (2008), Wiseman et al. (2012), Yue et al. (2010). The red arrow indicates the plate motion of Australian and Indian plates relative to Sunda plate which estimated by the GSRMv2.1 plate motion model of Kreemer et al. (2014). The colored rupture patches of large interplate earthquakes illustrated the slip areas > ~2 m. Background bathymetry/topography is from GEBCO (Kapoor 1981). AU: Australian Plate, SU: Sunda Plate, GSF: Great Sumatran Fault.

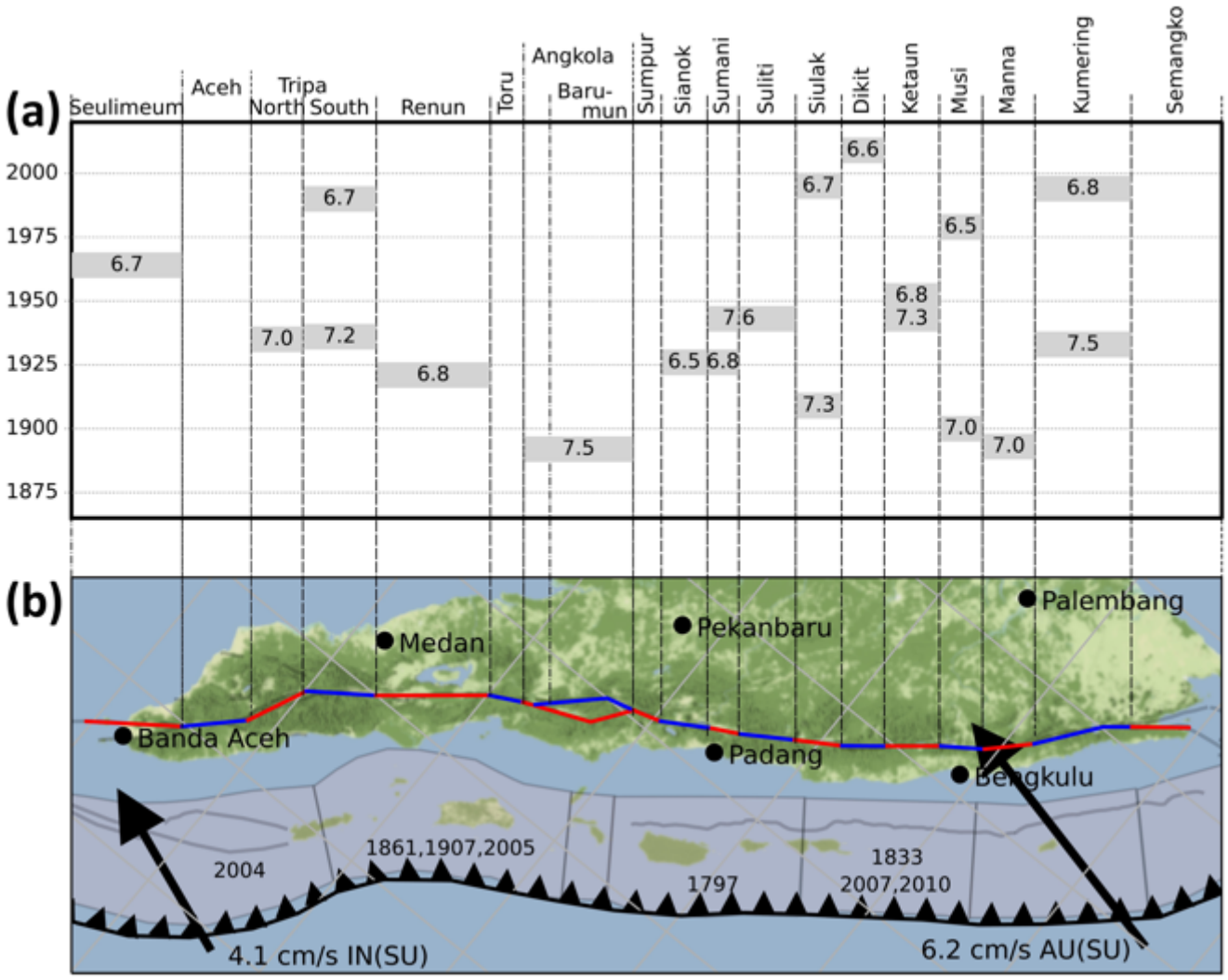

Figure 2

The 19 segments of the Great Sumatran Fault (GSF) and the GSF earthquakes as described by Hurukawa et al. (2014), along with GSF trace data and subduction megathrust segments from Irsyam et al. (2020). Note that the bifurcations of the GSF in the north and south, where the Seulimeum/Aceh and Semanko West/East segments overlap, respectively have been simplified to consider only the Seulimeum and Semangko West (referred here simply as Semangko) segments, since they are most favourably oriented with respect to the stress field. Also, the Tripa segment of Hurkawa et al. (2014) has been split into Tripa North and Tripa South segments, to better conform to the surface trace of the GSF as given in Irsyam et al. (2020). GPS vectors of Australian and Indian Plate motion relative to the Sunda Black are from Kreemer et al. (2014).

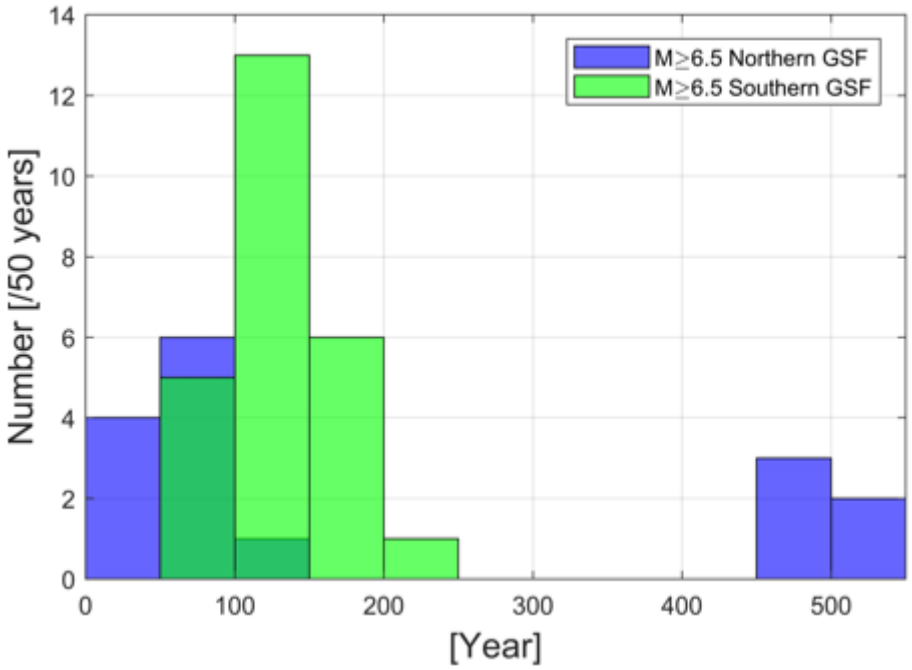

Figure 3

Histogram of the time intervals between the occurrence of each GSF earthquake in Table 1 and all preceding megathrust events that occurred with 500 km of the GSF event. The origin of the horizontal axis, year 0, corresponds to the occurrences of the great Sumatra megathrust earthquakes in 1450, 1797, 1833, 1861, 1907, 2004, 2005, 2007 and 2010. GSF earthquakes have been split into northern GSF events, consisting of ruptures of the Seulimeum, Renun, Tripa and Angkola segments, and southern GSF events, consisting of ruptures of the Sumani, Sianok, Suliti, Siulak, Dikit, Ketaun, Musi, Manna and Kumering segments.

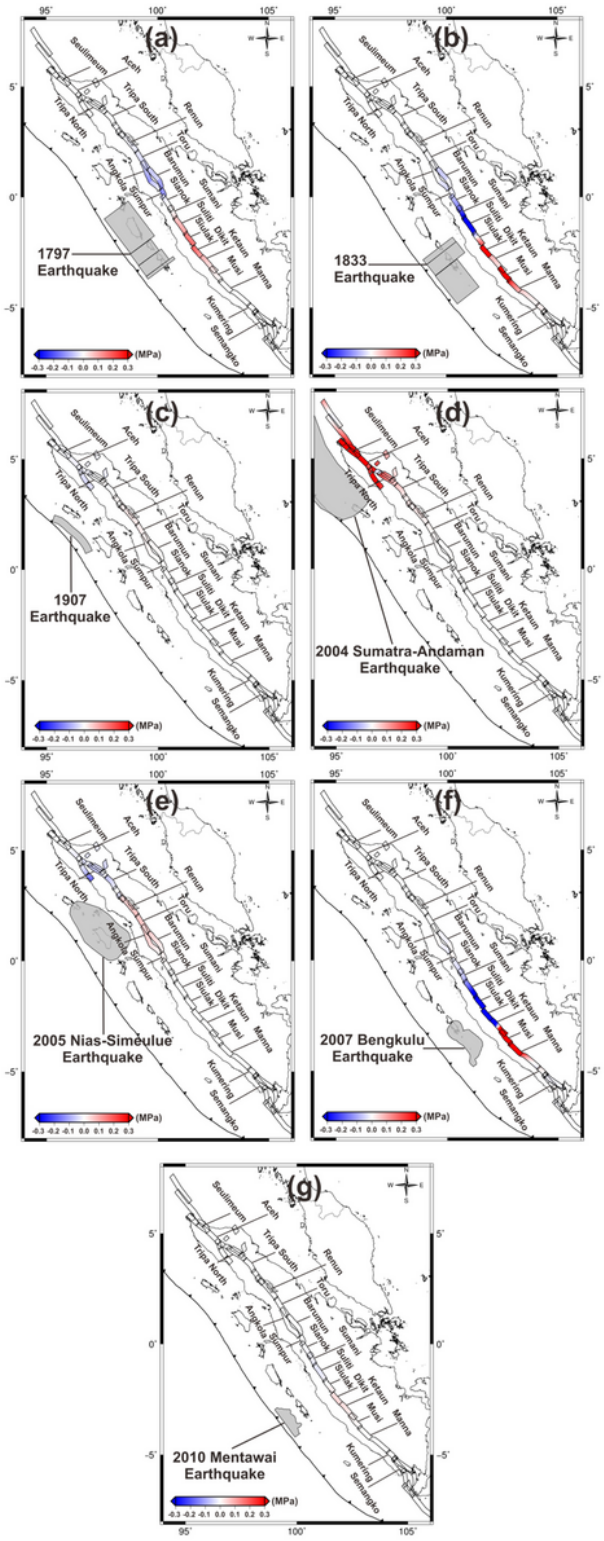

Figure 4

Static coseismic ΔCFS_m of megathrust earthquakes calculated at 10 km depth with a scale saturated at 3 bars. (a) ΔCFS_m of 1797 earthquake, (b) ΔCFS_m of 1833 earthquake, (c) ΔCFS_m of 1907 earthquake, (d) ΔCFS_m of 2004 Sumatra-Andaman earthquake, (e) ΔCFS_m of 2005 Nias-Simeulue earthquake (similar to 1861 earthquake), (f) ΔCFS_m of 2007 Mentawai earthquake, and (g) ΔCFS_m of 2009 Padang

earthquake, and (h) ΔCFS_m of 2010 Mentawai earthquake. The grey polygon is the rupture area of megathrust earthquake.

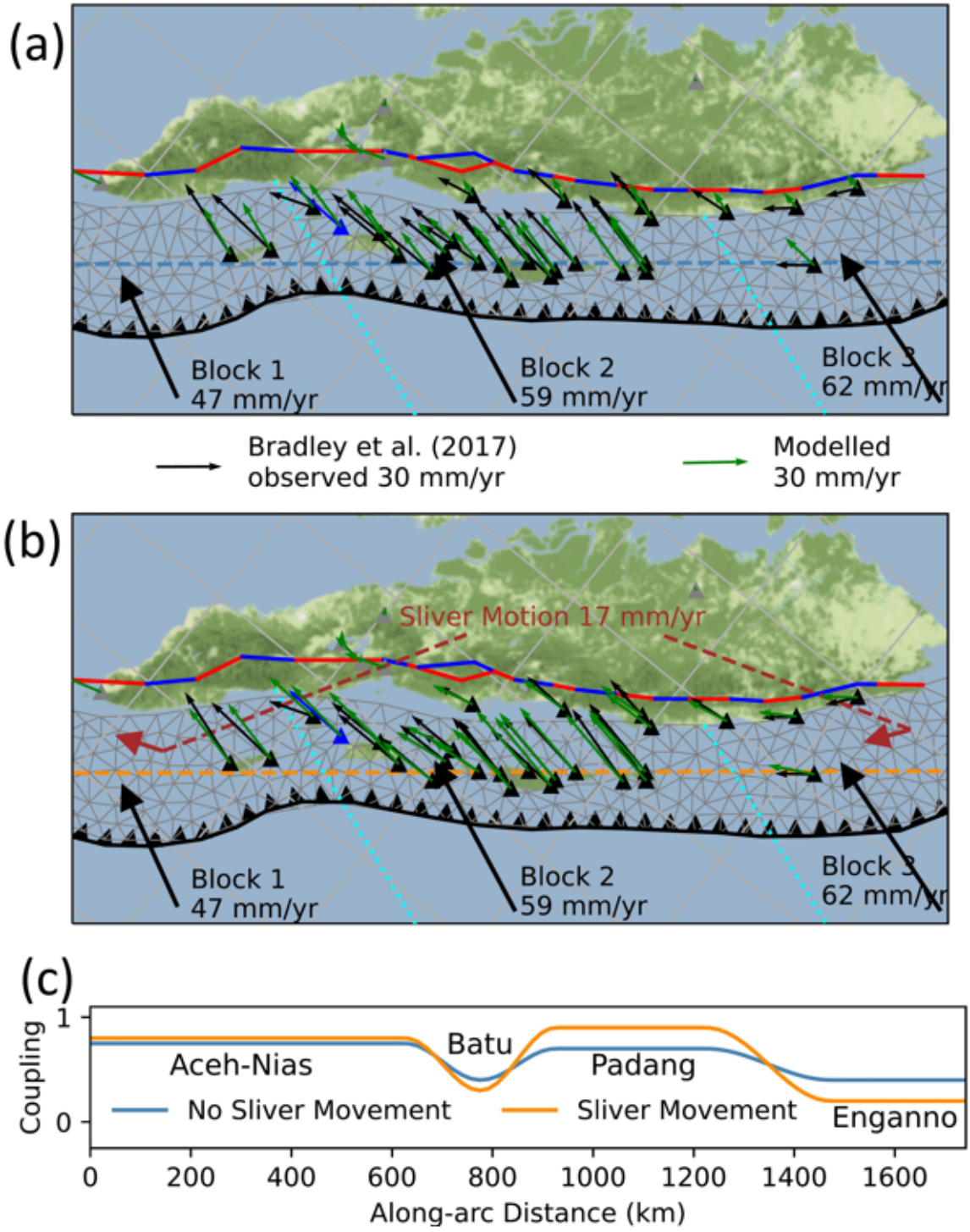

Figure 5

Modelling of GPS data from Bradley et al. (2017) for megathrust coupling models (a) with and (b) without (b) forearc sliver movement. In both (a) and (b), the triangular elements used to tesselate the

Sumatra megathrust model of Hayes et al. (2018) are displayed, as is a comparison of modelled GPS velocities (green arrows) and observed velocities used for the kinematic modelling of Bradley et al. (2017, black arrows). (c) shows profiles of the megathrust coupling obtained by optimising the fit of the GPS data for the two cases of no sliver movement and sliver movement in (a) and (b), respectively. In order to fit the data for each case, coupling values were varied in the Aceh-Nias, Batu, Padang and Enggano portions of the Sumatra megathrust.

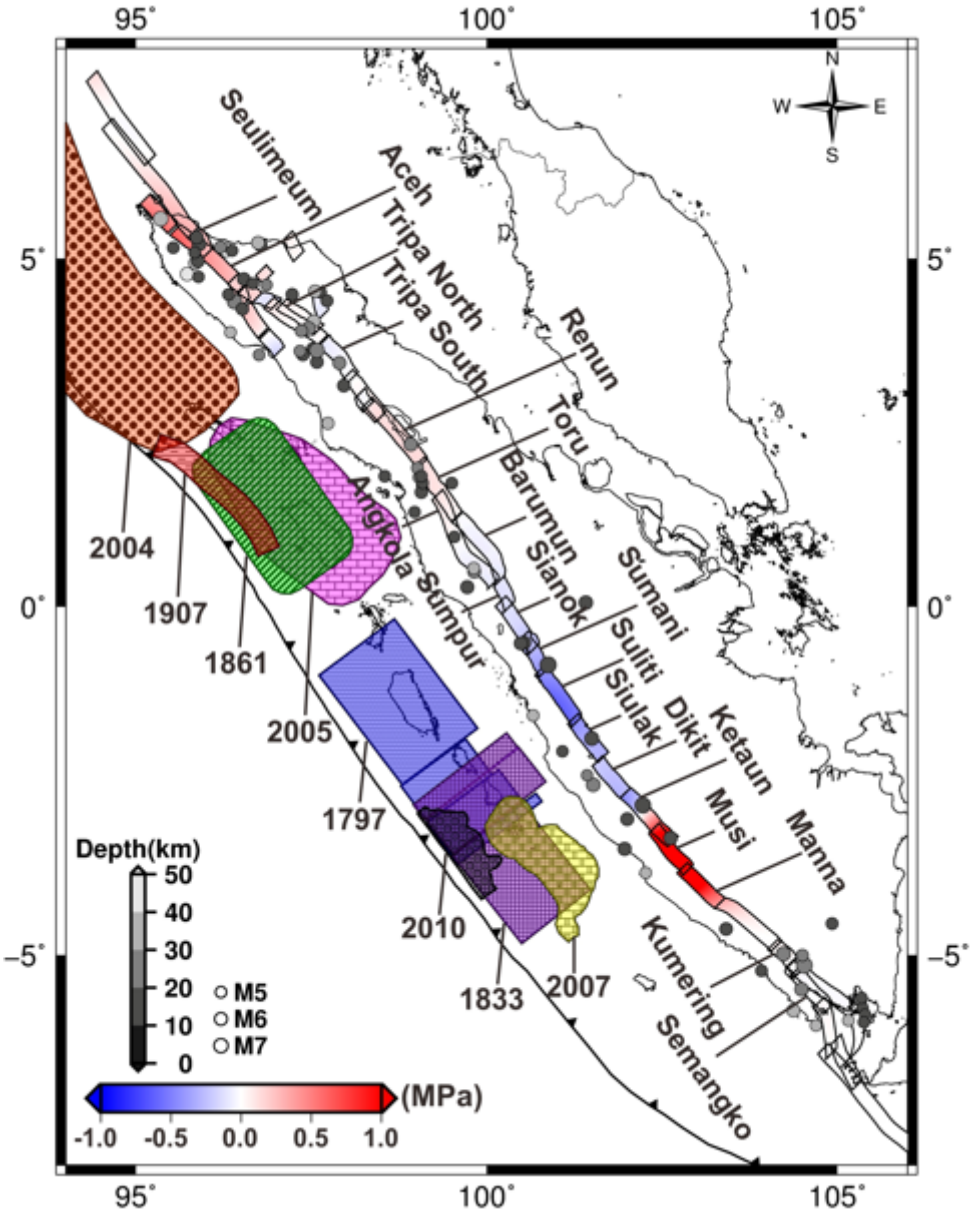

Figure 6

Map of cumulative ΔCFS_m from 8 megathrust earthquakes (1797-2010 earthquakes) on the GSF. The pattern-colored polygons are the rupture areas of each megathrust earthquake adapted from previous studies. The grey circles indicate seismicity from 1909 to 2015 from ISC-GEM catalogue (Di Giacomo et al. 2018; Storchak et al. 2015).

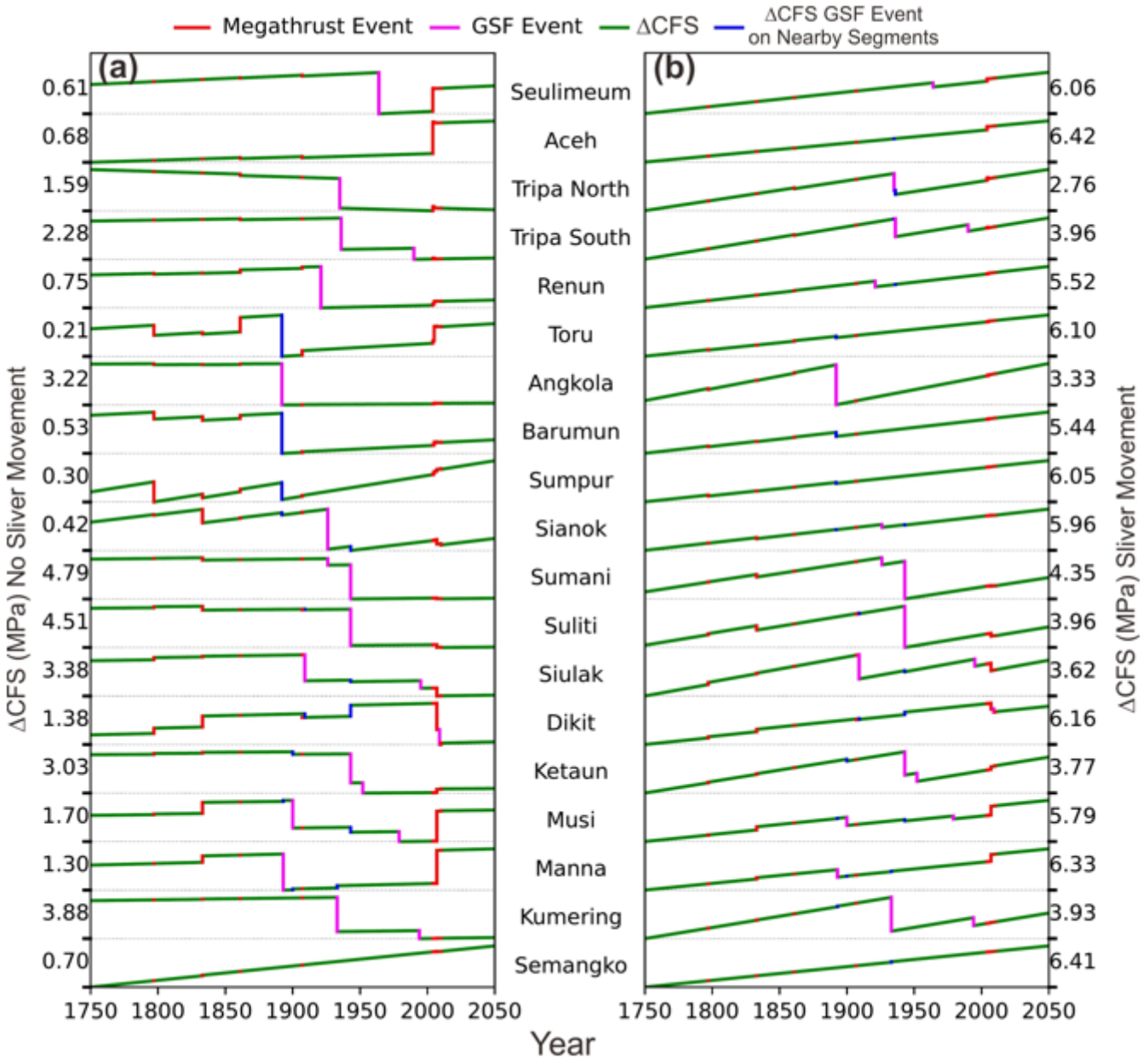

Figure 7

Time evolution of Coulomb stress change on each GSF segment, for the case (a) without arc-parallel movement of the forearc sliver, and (b) with arc-parallel sliver movement. Co-seismic changes in CFF due to the occurrence of megathrust (red) and GSF earthquakes (magenta for same segment, blue for adjacent segments) are indicated. The total change in CFS accumulated over the years 1750-2050 for each segment is indicated on the left of (a) and the right of (b). Note, however, that the poor availability of historical records in the early to mid-19th century means that some segment ruptures may have been missed, resulting in over-estimate of the accumulated ΔCFS.